Hindawi
International Journal of Antennas and Propagation
Volume 2021, Article ID 9795959, 12 pages
https://doi.org/10.1155/2021/9795959

Research Article

Design of a Novel 60 GHz Millimeter Wave Q-Slot Antenna for Body-Centric Communications

Mohammad Monirujjaman Khan,[1] **Kaisarul Islam**,[1] **Md. Nakib Alam Shovon**,[1] **Mohammed Baz**,[2] **and Mehedi Masud**[3]

[1]*Department of Electrical and Computer Engineering, North South University, Dhaka-1229, Bangladesh*
[2]*Department of Computer Engineering, College of Computers and Information Technology, Taif University, P.O. Box 11099, Taif 21944, Saudi Arabia*
[3]*Department of Computer Science, College of Computers and Information Technology, Taif University, P.O. Box 11099, Taif 21944, Saudi Arabia*

Correspondence should be addressed to Mohammad Monirujjaman Khan; monirujjaman.khan@northsouth.edu

Received 16 August 2021; Accepted 18 October 2021; Published 2 November 2021

Academic Editor: Ana Vazquez Alejos

The 60 GHz band is a great prospect to meet the future demand for short-range indoor communication requiring wide bandwidth and high data rates. This paper presents the design of a 60 GHz printed Q-slot patch antenna for body-centric communication. The Q-slot has a slot gap of 0.2 mm and is etched on a 6.5 mm × 11 mm rectangular patch. The slotted patch is mounted on an FR-4 (Flame Retardant) substrate that is 1.6 mm thick and has a relative permittivity of 4.3. With a partial ground plane of length of 2.2 mm, the antenna's overall dimension is 12.9 mm × 14 mm × 1.6 mm. Computer Simulation Technology (CST) microwave studio was used to design and simulate the antenna. In free space, the antenna is resonant at 60.06 GHz with an impedance bandwidth of 12.11 GHz. At 60 GHz, the antenna's radiation efficiency is 82.15%, with a maximum gain of 8.62 dBi. For further analysis, parametric changes were made to observe the effect on return loss, radiation efficiency, and gain. The antenna was simulated on a three-layer human torso phantom for the on-body scenario. The antenna's resonant frequency shifted slightly to the right at 2 mm distant from the phantom while maintaining a very wide impedance bandwidth. At this point, the antenna's radiation efficiency dropped to 56.68% and gradually increased to 74.04% at 10 mm. The maximum gain remained largely unaffected, but some grated radiation patterns were observed.

1. Introduction

The WBAN is a network of sensors that work in the human body's vicinity to collect important data. A part of the emerging body-centric wireless communication (BCWC) technology, WBAN plays an important role in today's wearable devices. Current wireless systems, such as WBAN, Wireless Local Area Network (WLAN), and Wireless Personal Area Network (WPAN), work under 10 GHz of the electromagnetic spectrum. With the increased usage of wireless devices, it is evident that these systems are getting congested and will suffer in the future from a lack of bandwidth. Consequently, we are already witnessing wireless communication systems shifting to the millimeter wave (mmWave) spectrum. The mmWave spectrum expands from 30 GHz to 300 GHz, providing wide bandwidth, high data rates (in the Gbps range), and high security. The 60 GHz band, a part of the mmWave spectrum, is largely unlicensed around the world. Atmospheric absorption of mmWave is highest at 60 GHz due to resonance with oxygen molecules, making it suitable only for short-range communication. On the other hand, high atmospheric absorption provides good security as signals are more difficult to interfere with [1]. For short-range indoor WBAN systems, the 60 GHz band is a promising solution. The Federal Communications Commission (FCC) approved the 57–64 GHz band for unlicensed usage in 2001. The Institute of Electrical and Electronics Engineers (IEEE) published the IEEE802.11ad standard in

2012 to promote WLAN technologies operating in the 60 GHz (57.24–70.20 GHz) band. The standard enables data rates up to 7 Gbps for a maximum distance of 12 m [2, 3]. This prompted the development of many 60 GHz antenna designs that will meet the future demand for high bandwidth systems [4–10].

Microstrip patch antennas are low-profile, compact, and easy-to-fabricate antennas that are suitable for mmWave communication systems. One major disadvantage of using microstrip patch antennas is their narrow bandwidth. To counter this problem, many researchers have introduced slots on the patch. The slots not only enhance the bandwidth but also reduce the patch size and enhance efficiency. In [11], the authors introduced two rectangular slots for a 28 GHz 5G antenna. With the introduction of the slots, the bandwidth increased from 1.46 GHz to 2.26 GHz. The antenna maintained stable gain ranging from 7.1 to 7.65 dBi over the whole operating band. Various designs of MIMO antennas and techniques, reconfigurable, tunable, and array antennas for different applications, are presented in [12–20]. A U-slot microstrip patch antenna for the 28 GHz band is presented in [21]. The antenna achieved a relative bandwidth of 21.92% and demonstrated a radiation pattern with a 100° beamwidth. A dual-band circularly polarized slotted patch antenna consisting of L-shaped slots has been proposed in [22]. The L-shaped slots around the patch add capacitive and inductive effects, resulting in multiple resonant frequencies at 28 and 38 GHz. The slots lengthen surface currents, which reduces the patch size and causes the lower resonant frequency to shift to the left. A small T-slot microstrip antenna for mmWave communication is presented in [23]. The antenna meets the IEEE802.11ad standard by operating in the 60 GHz band with a maximum gain of 6.34 dB. Another slotted patch antenna designed for 30 GHz operation demonstrated tri-band characteristics by introducing two narrow linear slots [24]. Even though the mentioned works are designed for lower band operation, there are also a few examples of 60 GHz slotted patch antennas. A single band antenna consisting of E and H-shaped slots for bandwidth enhancement has been proposed in [25]. Wu et al. presented a high gain E-shaped patch antenna array in [26]. The antenna's bandwidth ranged from 56.6 to 64.5 GHz. A rectangular patch antenna consisting of a U-shaped slot with unequal arms has been proposed in [27]. The unequal arms act as coupled resonators that widen the bandwidth by shifting the resonant frequency towards lower and higher frequencies. The antenna's reported bandwidth is 15.4 GHz, covering 52.20 GHz to 67.70 GHz with a gain of 9.52 dB. No on-body (antenna placed close to a human body) results are reported for these works. For 60 GHz body-centric communication, it is important to evaluate the antenna for the on-body scenario. An antenna's efficiency, bandwidth, and radiation patterns are affected by the lossy nature of the human body. To study the effect of the human body on the 60 GHz antenna, a microstrip patch antenna was proposed in [28]. When the antenna was put close to a human body phantom, its efficiency was reduced by 10% compared to free space. A 2% efficiency drop of a microstrip four patch array antenna is reported in [29]. An end-fire Yagi-Uda and a horn antenna's efficiency decreased by 30% [30, 31]. The on-body gain increased by almost 2 dBi in these reported works. In [29], a horn antenna's efficiency dropped by 40% and saw its gain decrease by 2 dBi.

Yeboah-Akowuah presented a printed monopole rectangular antenna in [32] for UWB on-body operation. The patch of the antenna consists of a Q-shaped slot that has been optimized through the Trust Region Framework (TRF) algorithm. The slot improved the antenna's efficiency, gain, and bandwidth. In [33], Khan et al. proposed a textile-based compact antenna for body-centric communication. For the proposed design, many textile substrates have been used and compared. In this paper, we are proposing a design for the Q-slot antenna for the unlicensed 60 GHz band. The antenna includes the substrate, ground plane, and radiating element. The slot gap, rectangular patch, and partial ground will be optimized to operate in the mmWave range. Parametric studies will be conducted to analyze how the antenna's bandwidth, radiation efficiency, and gain are affected. Lastly, the antenna will be simulated on a human torso phantom for on-body performance evaluation. The paper will focus on simulation results only. The CST Microwave Studio will carry out the design and simulation process of the antenna.

Including the introduction and conclusion, this paper is divided into six different sections. The design of the antenna is described in Section 2. Section 3 shows the antenna's free space results. Sections 4 and 5 discuss the parametric and on-body results, respectively. Section 6 concludes this study.

2. Design of the Antenna

The wavelength in the mmWave range is very small. At 60 GHz, the wavelength is just 5 mm. This allows the antenna design to be much smaller in size compared to its lower band counterparts. The antenna is built on an FR-4 substrate with a relative permittivity of 4.3. The substrate measures 12.9 mm × 14 mm × 1.6 mm. The electrical size of the proposed antenna at 60 GHz for the length and width is 0.769λ and 0.454λ, respectively. A partial ground with a length of 2.2 mm is attached to the bottom of the substrate. The radiator patch is placed on top of the substrate and measures 6.5 mm × 11 mm. The patch consists of a Q-slot, which is made by carving a circular and rectangular slot. The outer radius ("r") of the circular slot is 2.2 mm, and the width of the rectangular slot is 2 mm (denoted by "t"). An overall slot gap of 0.2 mm is maintained. The antenna is fed by a 0.7 mm wide 50 Ω microstrip feedline. The position of the feedline is 2.2 mm away from the right-hand side of the radiating patch and is denoted by "p." Figures 1(a)–1(g) show different views of the antenna. The various parts of the antenna are letters marked in Figures 1(a) and 1(b). The details of these markers are given in Table 1. Table 2 contains the material details of the antenna.

3. Free Space Simulation Results

The return loss curve (Figure 2) shows that the antenna has two resonant frequencies when the free space simulation runs from 50 to 70 GHz. The first resonant frequency is at

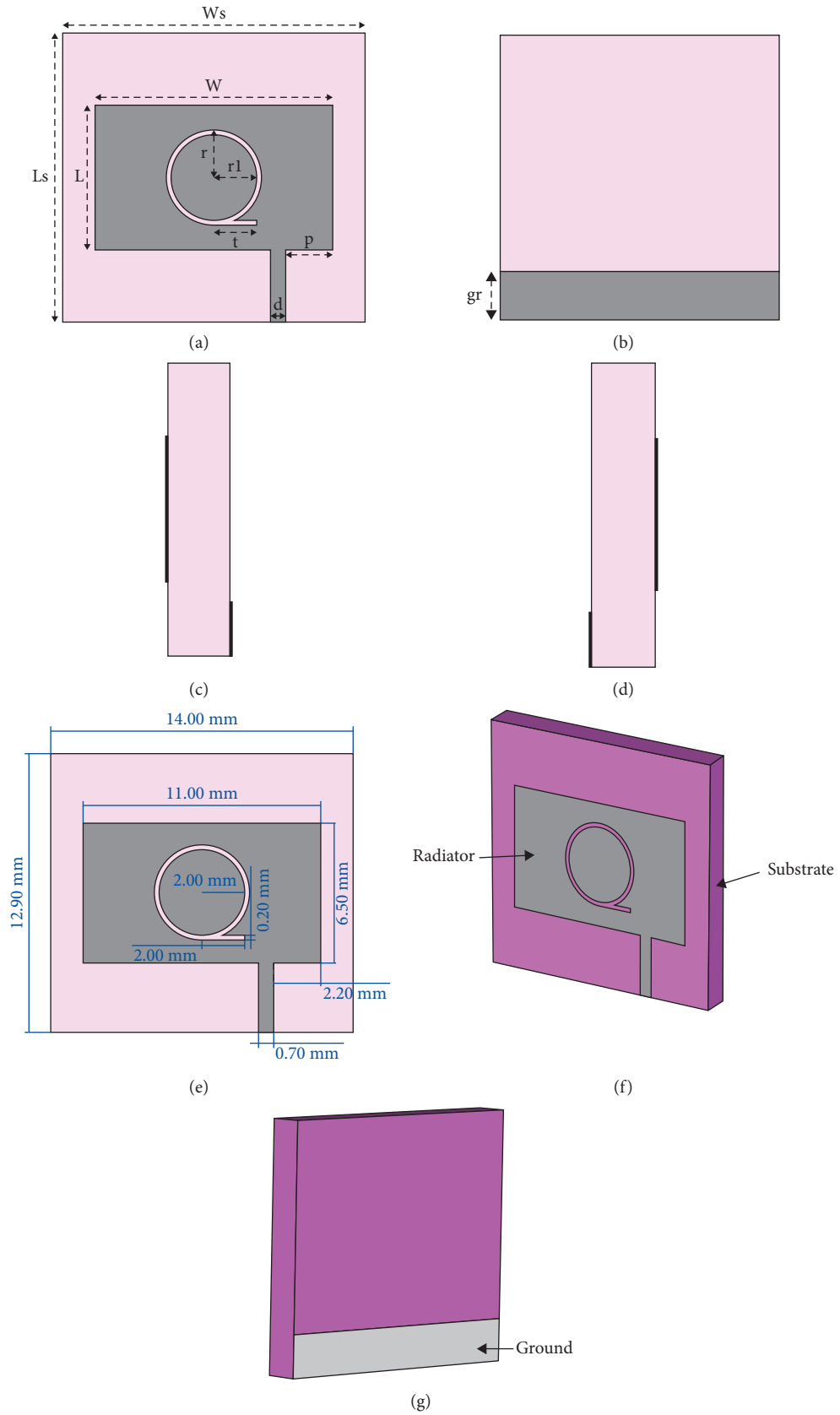

Figure 1: Proposed antenna design. (a) Top view, (b) back view, (c) right view, (d) left view, (e) antenna dimensions, (f) perspective front view, and (g) perspective back view.

Table 1: Antenna dimensions.

Parameter	Description	Value (mm)
Ls	Substrate length	12.9
Ws	Substrate width	14
L	Radiator length	6.5
W	Radiator width	11
d	Substrate thickness	0.7
gr	Ground length	2.2
p	Feedline position	2.2
r	Outer radius	2.2
$r1$	Inner radius	2
t	Q descender	2

Table 2: Antenna materials.

Parameter	Thickness (mm)	Material	Relative permittivity
Ground	0.035	PEC	—
Patch radiator	0.035	PEC	—
Substrate	1.6	FR-4	4.3

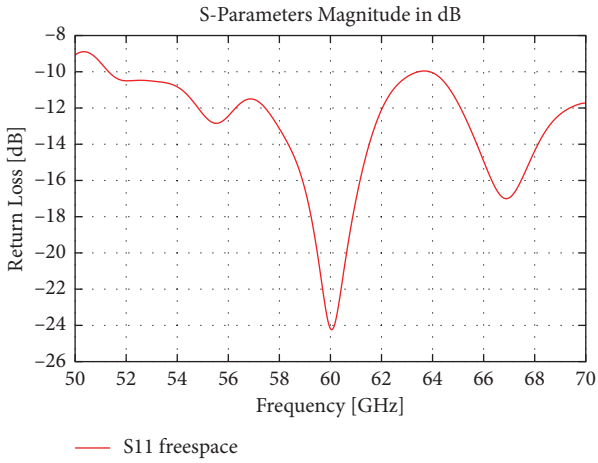

Figure 2: S-parameters for free space.

60.06 GHz with a −10 dB impedance bandwidth of 12.11 GHz. The antenna's radiation efficiency is 82.15% at this resonant frequency, with a maximum gain of 8.62 dBi. Figures 3(a)–3(c) show the radiation patterns of the antennas. The E-plane radiation pattern demonstrates good beamwidth with some grated side lobes (Figure 3(b)). On the other hand, the H-plane radiation pattern shows a very narrow beamwidth (Figure 3(c)). The free space (three-dimensional) 3D radiation pattern at 60 GHz in Figure 3 shows that radiation is mostly directed along the y axis. The surface current distribution (Figure 4) shows an increased amount of surface current around the slot. The voltage standing wave ratio (VSWR) measures the amount of energy reflected back to the source. The ideal value of VSWR is 1, which means no energy is reflected back. In some instances, VSWR equaling 2 is acceptable, indicating that only 10% of the energy is reflected back to the source. A value of less than 1.5 is desirable. The proposed design's VSWR is very close to 1 at resonant frequencies and remains below 2 over the whole simulated range (Figure 5).

4. Parametric Study

Parametric studies of the antenna have been carried out by varying different parameters one at a time. For the analysis, the feedline width "d," feedline position "p," and slot gap have been changed to observe how the return loss curve, efficiency, and gain are affected.

4.1. Feedline Width ("d"). When the width of the feedline (denoted by "d") was changed to 0.9 mm, the shape of the return loss remained similar to the final design. The lower end of the frequency bandwidth shifted slightly to the left and the antenna covered beyond the whole simulated frequency range. Compared to the final design, the first resonant frequency shifted to 59.92 GHz. A negligible increase in maximum gain was observed, while the radiation efficiency was on par with free space value. For a feedline width of 0.5 mm, the −10 dB impedance bandwidth decreased, and a dual-band characteristic was observed. The resonant frequencies shifted slightly to the right side. For a center frequency of 60.12 GHz, the antenna achieved an impedance bandwidth of 9.66 GHz. The return loss curves for different "d" values are given in Figure 6(a). The radiation efficiency and gain at this resonant frequency decreased compared to the final design. The simulation results are summarized in Table 3.

4.2. Feedline Position ("p"). Similar to feedline width, the feedline position "p" has a similar effect on the return loss curve. When the distance between the edge and the feedline decreased, we observed dual-band characteristics. At the resonant frequency of 60.06 GHz, the impedance bandwidth decreased to 11 GHz. The radiation efficiency increased by more than 1%, but the maximum gain decreased slightly. The opposite was observed for an increased distance of "p." The antenna's resonant frequency shifted left to 59.98 GHz. The impedance bandwidth covers most of the frequency range the antenna was simulated on. The results are detailed in Table 4. In Figure 6(b), the return loss curves are depicted for comparison.

4.3. Ground Length ("gr"). A smaller ground length shifted the resonant frequency from 60.06 GHz to 58.94, while a larger ground length shifted the frequency to 61.4 GHz. The return loss curve for a ground length of 2.5 mm shows a triband characteristic (Figure 6(c)). The impedance bandwidth for a ground length of 2 mm is well above 20 GHz. Changing the ground length significantly affected maximum gain at resonant frequencies, while the radiation efficiencies increased in both cases. Table 5 shows the detailed values.

4.4. Slot Gap. The final design of the antenna has a slot gap of 0.2 mm. For parametric analysis, we changed the size of the slot gap to 0.3 mm and 0.1 mm. The gap can be altered by either changing the size of the parameters "r" or "$r1$." For example, the slot gap can be increased to 0.3 mm by either increasing the size of "r" to 2.3 mm or by decreasing the size

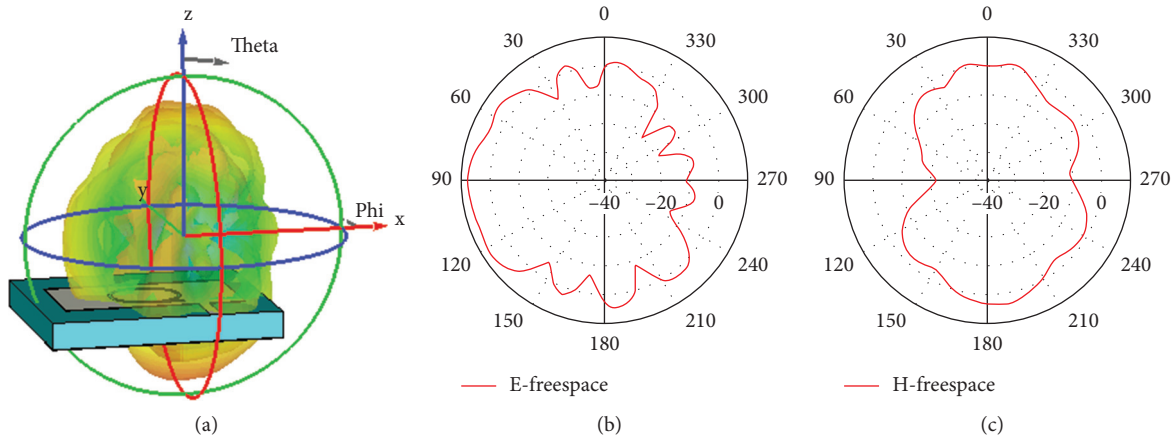

Figure 3: (a) 3D radiation pattern free space for 60 GHz, (b) E-plane radiation pattern free space for 60 GHz, and (c) H-plane radiation pattern free space for 60 GHz.

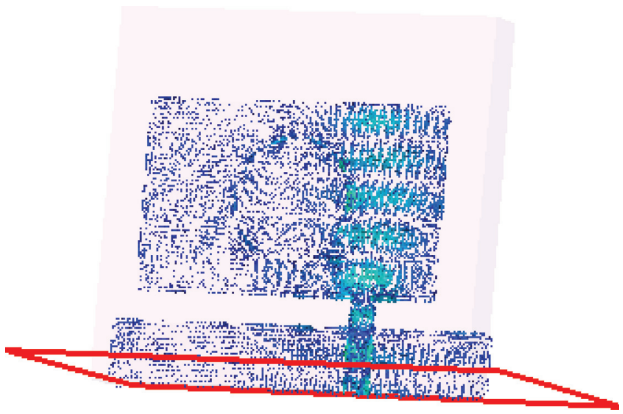

Figure 4: Surface current free space for 60 GHz.

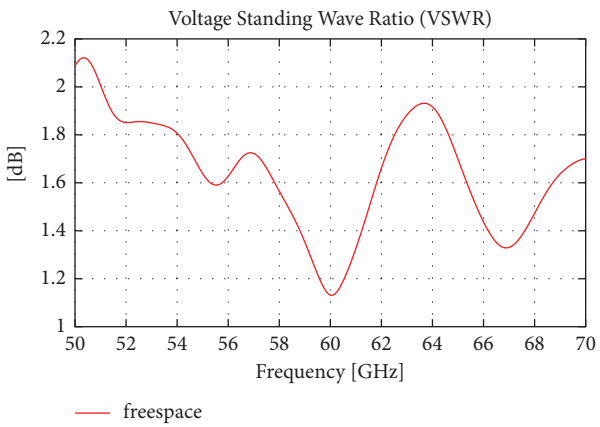

Figure 5: VSWR for free space at 60 GHz.

of "$r1$" to 1.9 mm. Subsequently, the slot size can be decreased to 0.1 mm by either decreasing or increasing the size of "r" or "$r1$" to 2.1 mm, respectively. For a slot gap of 0.1 mm, the impedance bandwidth was around 11.7 GHz, with a resonant frequency slightly higher than 59.9 GHz. At this frequency, the maximum gain was around 8.89 dBi with a radiation efficiency of more than 82%. For a slot gap of 0.3 mm, the "r" value is 2.3 mm, or the "$r1$" value is 1.9 mm. For an "r" value of 2.3 mm, the antenna was resonant at 60.28 GHz, and for an "$r1$" value of 1.9 mm, the antenna was resonant at 60.12 GHz. The maximum gain was comparable to the final design, while the radiation efficiency was slightly less at around 81%. Table 6 summarizes the antenna's performance for different slot gaps by varying either "r" or "$r1$." See Figures 6(d) and 6(e) for a comparison of return loss curves for different "r" and "$r1$" values.

5. On-Body Simulation Results

The millimeter wave's penetration depth into the human body is quite low. A human torso phantom can be modeled in CST to evaluate the effect of the antenna's performance in proximity to the human body. The phantom consists of the three outermost layers of the human body—skin, fat, and muscle (Figure 7). The dimension, relative permittivity, and conductivity of these layers are given in Table 7 [34]. At 60 GHz, the wave can penetrate only 0.48 mm of skin. For this reason, most of the 60 on-body antenna designs are evaluated on a 2 mm thick skin phantom. For accuracy purposes, the proposed antenna has been evaluated on three layers. In real life, body-worn devices can be several millimeters away from humans. We have simulated this scenario by keeping the antenna five distances away from the phantom for a frequency range of 50 GHz to 85 GHz. Starting from 2 mm, the distance was increased by 2 mm up to 10 mm (Figures 8(a)–8(e)).

At 2 mm, the resonant frequency shifted to the right at 60.43 GHz compared to the free space frequency of 60.06 GHz. As the distance increased, the resonant frequency kept on shifting to the left, and at 10 mm away from the phantom, the resonant frequency was very close to the free space value. At 4 mm, the antenna was resonant at 60.21 GHz with an impedance bandwidth of 30.07 GHz (Figure 9). The 60 GHz 3D radiation pattern, polar plots (E and H), plane radiation, and surface current at this distance are given in 10–12. Like free space, the VSWR for all the distances is well below the acceptable value of 2 over the whole simulated range (Figure 13).

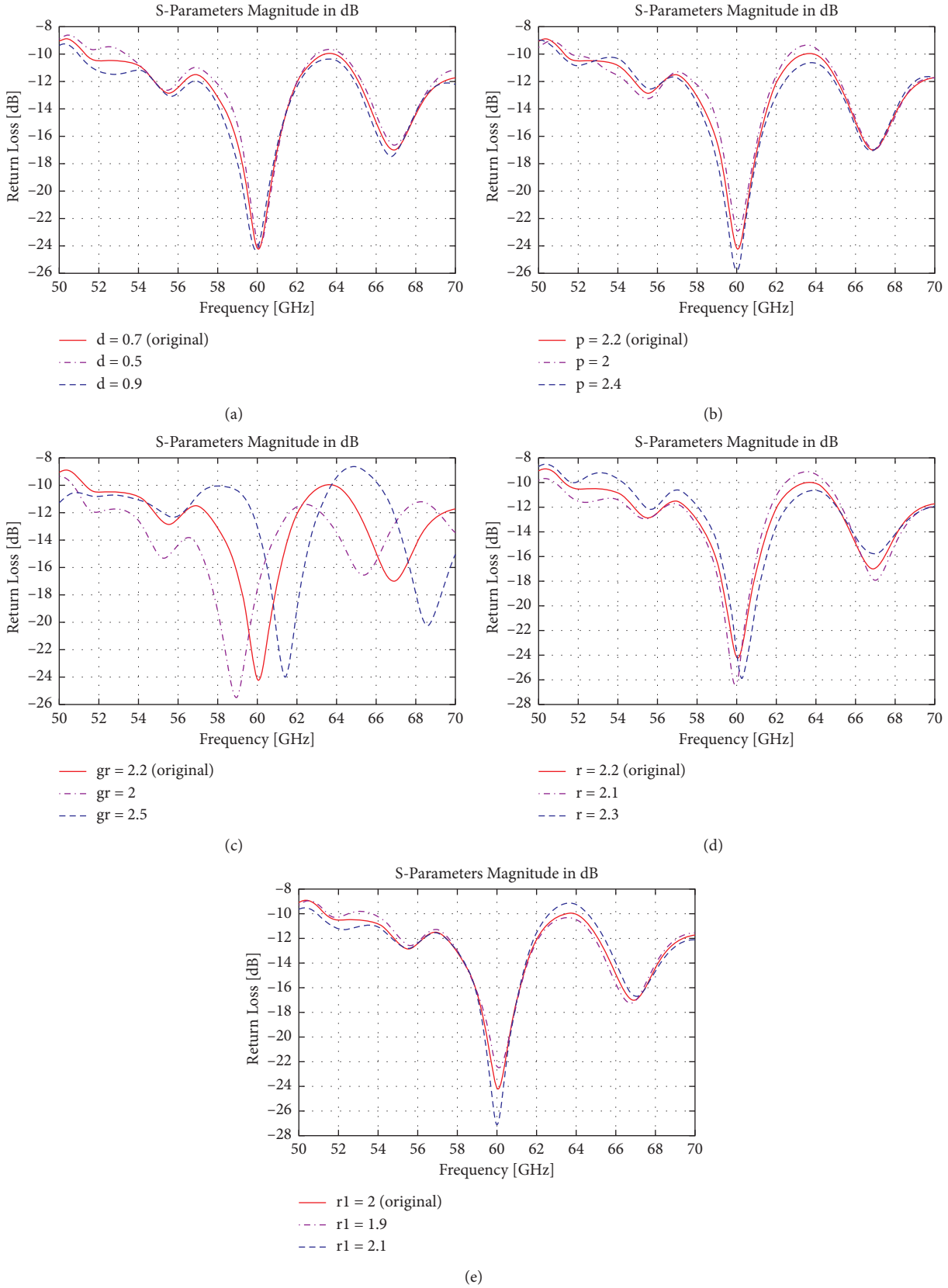

FIGURE 6: Return loss curve comparison for (a) different "d" values, (b) different "p" values, (c) different "gr" values, (d) different "r" values, and (e) different "$r1$" values.

Table 3: Feedline width "*d*" simulation summary.

Feedline width (mm)	Resonant frequency (GHz)	Bandwidth (GHz)	Gain (dBi)	Radiation efficiency (%)
0.5	60.12	9.66	8.39	82.07
0.7 (final design)	60.06	12.11	8.62	82.15
0.9	59.92	—	8.65	82.13

Table 4: Feedline position "*p*" simulation summary.

Feedline position (mm)	Resonant frequency (GHz)	Bandwidth (GHz)	Gain (dBi)	Radiation efficiency (%)
2	60.06	11.00	8.31	83.51
2.2 (final design)	60.06	12.11	8.62	82.15
2.4	59.98	—	8.69	80.88

Table 5: Ground length "gr" simulation summary.

Ground length (mm)	Resonant frequency (GHz)	Bandwidth (GHz)	Gain (dBi)	Radiation efficiency (%)
2	58.94	—	8.68	82.65
2.2 (final design)	60.06	12.11	8.62	82.15
2.5	61.4	—	8.67	81.79

Table 6: Length (ls) and width (ws) changes.

Parameters	Final design	$r = 2.1$	$r = 2.3$	$r1 = 1.9$	$r1 = 2.1$
Slot gap (mm)	0.2	0.1	0.3	0.3	0.1
Resonant frequency (GHz)	60.06	59.92	60.28	60.12	59.98
Bandwidth (GHz)	12.11	11.66	—	—	11.72
Gain (dBi)	8.62	8.89	8.40	8.47	8.88
Radiation efficiency (%)	82.15	82.09	81.74	81.27	82.49

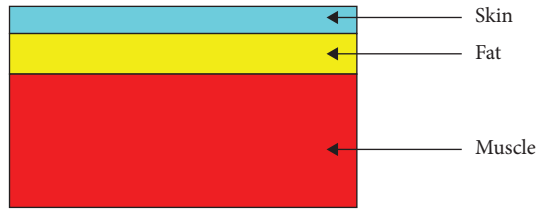

Figure 7: Torso phantom consisting of three outermost human body layers.

Table 7: Torso phantom physical characteristics.

Phantom layer	Length (mm)	Width (mm)	Thickness (mm)	Relative permittivity	Conductivity (S/m)
Skin	20	20	2	7.9753	36.397
Fat	20	20	3	3.1324	2.8152
Muscle	20	20	10	12.856	52.825

The antenna's free space and on-body return loss curves for various distances are shown in Figure 14. In the on-body case, due to different distances, the return loss curves vary. The radiation efficiency decreased quite significantly, especially very close to the phantom. This occurs as a result of the presence of a human body. When an mmWave antenna is placed on the human body, due to the lossy human body tissues, the radiation efficiency decreases. The lossy human tissues absorb the radiation power, which results in less radiation efficiency of this antenna when it is placed very close to the body. However, the effects are less when the gap between the antenna and the human body increases, as noticed from this study. At 2 mm, the efficiency dropped to 56.68% and gradually increased to 74.04% at 10 mm. The maximum gain was comparable to free space even though at 2 mm the value was less than 8 dBi. The radiation pattern showed no presence of major side lobes towards the phantom. Grated lobes were observed in both E and H

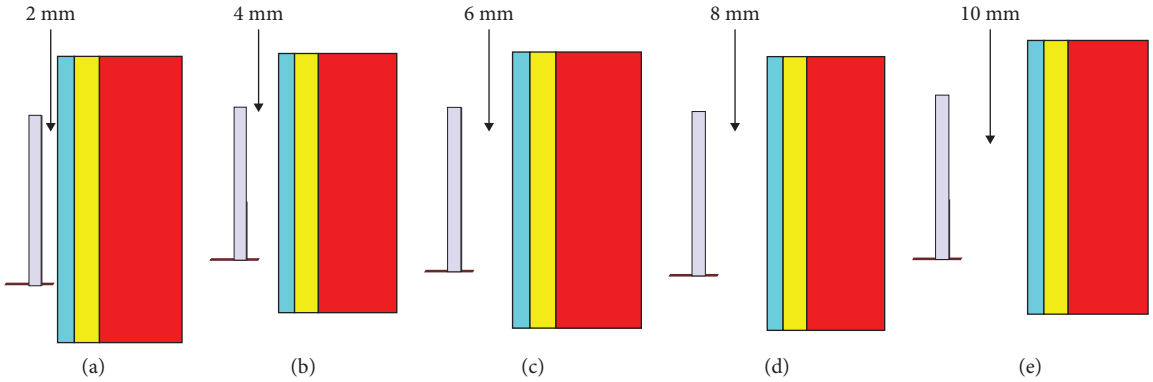

Figure 8: At five various distances from the phantom, a side view of the antenna on the body.

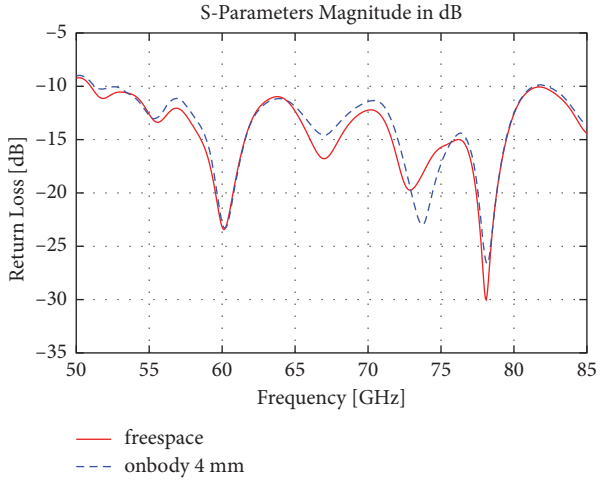

Figure 9: Return loss comparison between free space and on body.

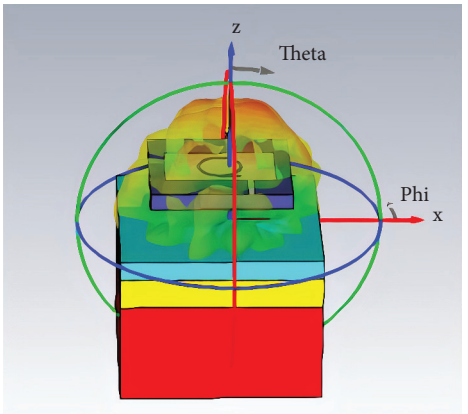

Figure 10: Far-field 3D radiation view on body 4 mm far with structure for 60 GHz.

planes and were more prevalent at 4 mm (Figure 11). As the distance between the antenna and the phantom increased, the radiation patterns were more similar to the free space pattern (Figure 15). The on-body simulation results are summarized in Table 8. A comparison of VSWR for different distances from the body and free space is shown in Figure 16.

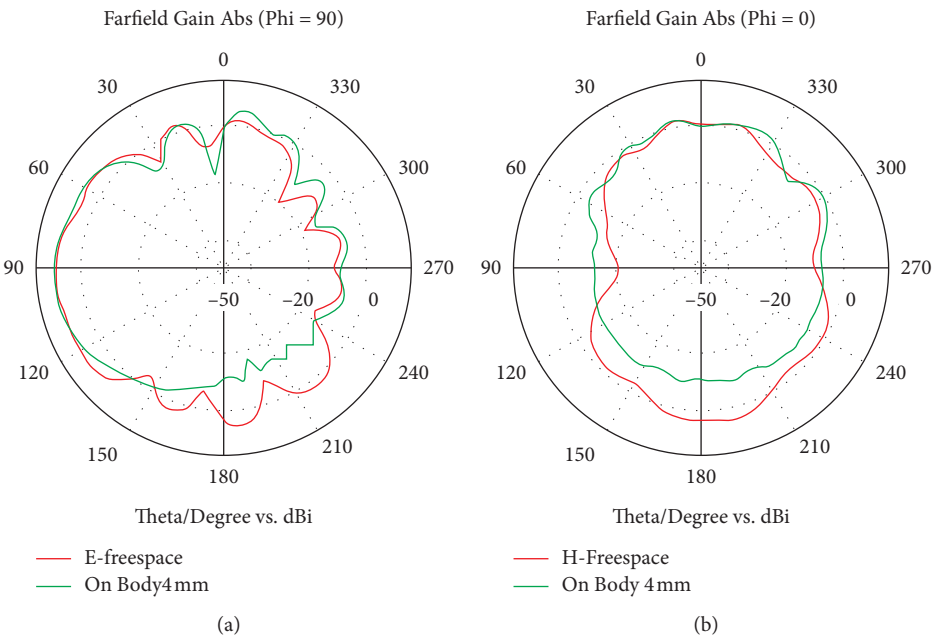

Figure 11: 60 GHz radiation pattern comparison at 4 mm. (a) E-plane and (b) H-plane.

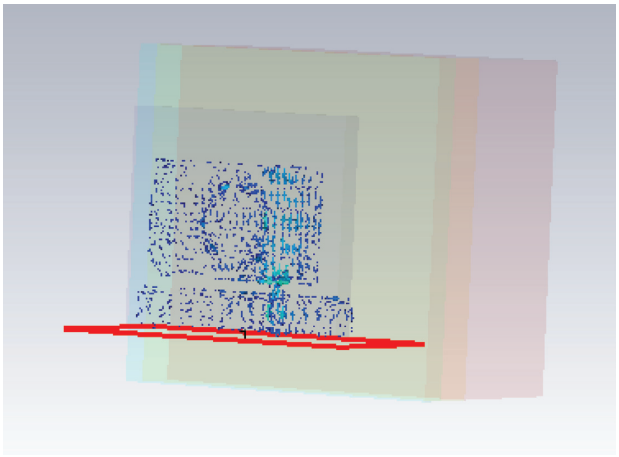

Figure 12: Surface current for 60 GHz on body (4 mm).

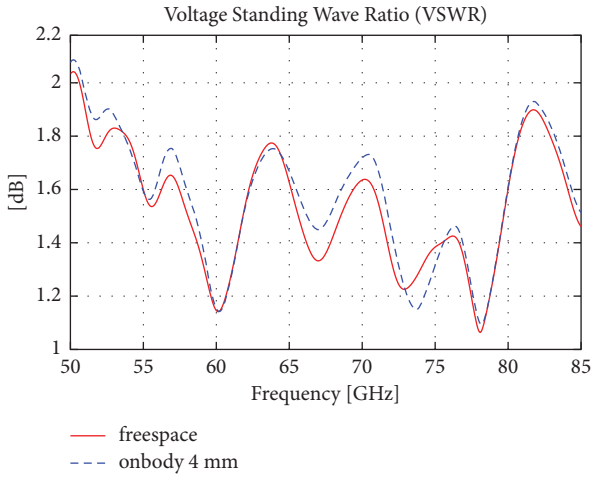

Figure 13: VSWR comparison for various on-body distances.

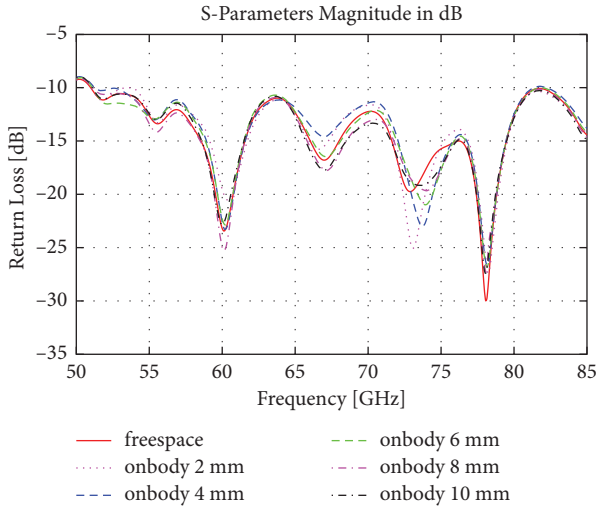

Figure 14: Return loss curves for free space and on body at different distances.

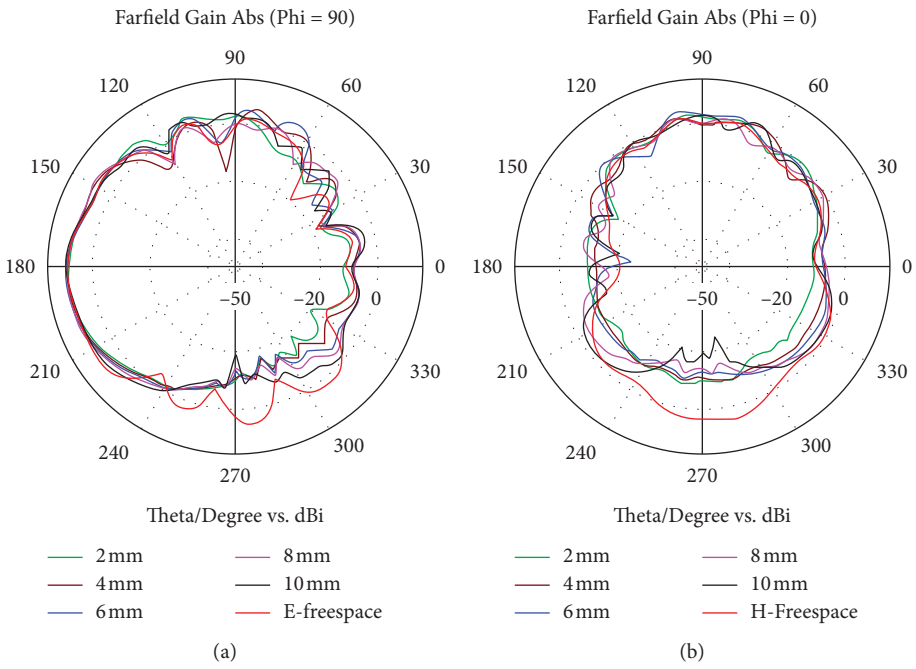

Figure 15: 60 GHz radiation pattern comparison for various on-body distances. (a) E-plane and (b) H-plane.

Table 8: Comparison parameters and results.

Parameters	Free space	On body 2 mm	On body 4 mm	On body 6 mm	On body 8 mm	On body 10m
Resonant frequency (GHz)	60.06	60.427	60.214	60.214	60.154	60.034
Bandwidth (GHz)	12.111	—	30.068	35.621	—	—
Gain (dBi)	8.617	7.926	8.660	8.423	8.108	8.291
Radiation efficiency (%)	82.15	56.68	67.79	70.31	73.12	74.04

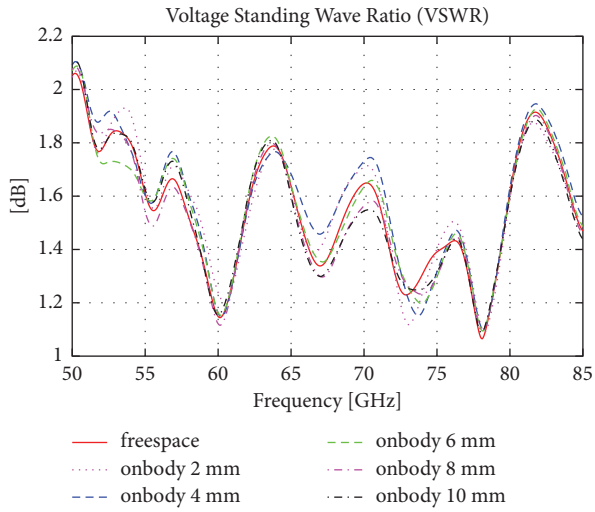

Figure 16: VSWR for 60 GHz on body at different distances.

6. Conclusion

The main purpose of this work was to design a suitable low-profile antenna for 60 GHz body-centric operation. The proposed antenna is smaller in size. Free space simulation and on body showed good impedance bandwidth covering the 60 GHz unlicensed band in every scenario. The bandwidth can be increased well beyond the 60 GHz band by increasing the slot gap, changing the feedline position, or changing the ground plane's length. On-body analysis of a human phantom showed good performance values. Some backward radiation towards the phantom caused the antenna's gain and radiation efficiency to drop. Overall, the antenna's performance is very good in free space and on-body scenarios. Even though the obtained results are not verified through experimental measurements, the CST simulation results can be relied upon as suggested in other works. The antenna would be a good design choice for future body-centric communications applications requiring good security and a high data rate in the short range.

In the future, the antenna can be designed on different textile substrates and study the performance of the antenna for body-centric communication. In addition, the size of the antenna can be optimized to operate on other frequency bands such as THz, GPS, and 2.45 GHz.

Data Availability

The data used to support the findings of this study are freely available at http://niremf.ifac.cnr.it/tissprop/.

Conflicts of Interest

The authors declare that they have no conflicts of interest to report regarding the present study.

Acknowledgments

The authors are thankful for the support from Taif University Researchers Supporting Project (TURSP-2020/239), Taif University, Taif, Saudi Arabia.

References

[1] J. F. Harvey, M. B. Steer, and T. S. Rappaport, "Exploiting high millimeter wave bands for military communications, applications, and design," *IEEE Access*, vol. 7, pp. 52350–52359, 2019.

[2] K. Islam, T. Hossain, and M. M. Khan, "A compact novel design of a 60 GHz antenna for body-centric communication," *International Journal on Communications Antenna and Propagation (IRECAP)*, vol. 10, no. 5, pp. 325–333, 2020.

[3] K. Islam, T. Hossain, M. Monirujjaman Khan, M. Masud, and R. Alroobaea, "Comparative design and study of a 60 GHz antenna for body-centric wireless communications," *Computer Systems Science and Engineering*, vol. 37, no. 1, pp. 19–32, 2021.

[4] B. Alexander and S. Daniel, "Pattern reconfigurable wideband stacked microstrip patch antenna for 60 GHz band," *International Journal of Antennas and Propagation*, vol. 2016, Article ID 5961309, 11 pages, 2016.

[5] R. Hoque, M. Asaduzzaman, I. Hossain, F. Imteaz, and U. Saha, "Distinguishing performance of 60-GHz microstrip patch antenna for different dielectric materials," in *Proceedings of the 2014 International Conference on Electrical Engineering and Information & Communication Technology*, pp. 1–4, Dhaka, Bangladesh, 2014.

[6] Y. Coulibaly, M. Nedil, L. Talbi, and T. A. Denidni, "Design of high gain and broadband antennas at 60 GHz for underground communications systems," *International Journal of Antennas and Propagation*, vol. 2012, Article ID 386846, 7 pages, 2012.

[7] J. Hautcoeur, L. Talbi, and K. Hettak, "Monopole lozange antenna for 60-GHz applications," in *Proceedings of the 2012 IEEE International Symposium on Antennas and Propagation*, pp. 1-2, Chicago, IL, USA, 2012.

[8] G. Zhang, S. Pu, X. Xu, Y. Liu, and C. Wang, "Design of 60-GHz microstrip antenna array composed through circular contour feeding line," in *Proceedings of the 2016 Asia-Pacific International Symposium on Electromagnetic Compatibility (APEMC)*, pp. 1010–1013, Shenzhen, China, 2016.

[9] D. Wang and C. H. Chan, "Multiband antenna for WiFi and WiGig communications," *IEEE Antennas and Wireless Propagation Letters*, vol. 15, pp. 309–312, 2016.

[10] L. Lu, K. Ma, F. Meng, and K. S. Yeo, "Design of a 60-GHz quasi-yagi antenna with novel ladder-like directors for gain and bandwidth enhancements," *IEEE Antennas and Wireless Propagation Letters*, vol. 15, pp. 682–685, 2016.

[11] Z. Li, R. Jian, Y. Chen, and T. Chen, "A novel design for millimeter wave microstrip antenna with bandwidth enhancement," in *Proceedings of the 2018 IEEE Student Conference on Research and Development (SCOReD)*, pp. 1–4, Selangor, Malaysia, 2018.

[12] P. Bactavatchalame and K. Rajakani, "Compact broadband slot-based MIMO antenna array for vehicular environment," *Microwave and Optical Technology Letters*, vol. 62, pp. 1–9, 2020.

[13] R. Rajmohan, K. S. Vishvaksenan, and R. Kalidoss, "Compact four port slot based MIMO antenna with isolation enhancement," *International Journal of Electronics*, vol. 108, no. 7, pp. 1–14, 2021.

[14] M. Saravanan, R. Kalidoss, B. Partibane, and K. S. Vishvaksenan, "Design of an interlocked four-port MIMO antenna for UWB automotive communications," *International Journal of Microwave and Wireless Technologies*, Cambridge University Press, Cambridge, UK, pp. 1–8, 2021.

[15] S. P. Damodaran, V. K. Srinivasan, and K. Rajakani, "Optimized and low-complexity power allocation and beamforming with full duplex in massive MIMO and small-cell networks," *The Journal of Supercomputing*, vol. 75, no. 12, pp. 7979–7993, 2019.

[16] B. Ashvanth, B. Partibane, M. Alsath, and R. Kalidoss, "Gain enhanced multipattern reconfigurable antenna for vehicular communications," *International Journal of RF and Microwave Computer-Aided Engineering*, vol. 30, no. 6, 2020.

[17] B. Ashvanth, B. Partibane, M. G. N. Mohammed, and K. Alsath, "Design of a 16-beam pattern-reconfigurable antenna for vehicular environment," *International Journal of RF and Microwave Computer-Aided Engineering*, vol. 13, no. 5, pp. 1–13, 2020.

[18] B. Ashvanth, B. Partibane, M. G. Nabi Alsath, and R. Kalidoss, "Tunable dual band antenna with multipattern reconfiguration for vehicular applications," *International Journal of RF and Microwave Computer-Aided Engineering*, vol. 29, no. 12, 2019.

[19] B. L. Dhevi, K. S. Vishvaksenan, and K. Rajakani, "Isolation enhancement in dual-band microstrip antenna array using asymmetric loop resonator," *IEEE Antennas and Wireless Propagation Letters*, vol. 17, no. 2, pp. 238–241, 2018.

[20] B. Partibane, M. Gulam Nabi Alsath, and K. Rajakani, "Design of a bandwidth enhanced hybrid slot loop antenna for GSM/UWB standards," *Circuit World*, vol. 43, no. 3, pp. 105–110, 2017.

[21] J. Xu, H. Ke, Y. He, and Y. Luo, "A wideband U-slot microstrip patch antenna for large-angle MMW beam scanning," in *Proceedings of the 2018 IEEE International Conference on Computer and Communication Engineering Technology (CCET)*, pp. 142–145, Beijing, China, 2018.

[22] H. Aliakbari, A. Abdipour, R. Mirzavand, A. Costanzo, and P. Mousavi, "A single feed dual-band circularly polarized millimeter-wave antenna for 5G communication," in *Proceedings of the 2016 10th European Conference on Antennas and Propagation (EuCAP)*, pp. 1–5, Davos, Switzerland, 2016.

[23] R. K. Goyal and K. K. Sharma, "T-slotted microstrip patch antenna for 5G Wi-Fi network," in *Proceedings of the 2016 International Conference on Advances in Computing, Communications and Informatics (ICACCI)*, pp. 2684–2687, Jaipur, India, 2016.

[24] K. Kumar and N. Gunasekaran, "A novel wideband slotted mm wave microstrip patch antenna," in *Proceedings of the 2011 International Conference on Signal Processing, Communication, Computing and Networking Technologies*, pp. 10–14, Thuckalay, India, 2011.

[25] J. Saini and S. K. Agarwal, "Design a single band microstrip patch antenna at 60 GHz millimeter wave for 5G application," in *Proceedings of the 2017 International Conference on Computer, Communications and Electronics (Comptelix)*, pp. 227–230, Jaipur, India, 2017.

[26] R. Wu, H. Tang, K. Wang, C. Yu, J. Wang, and X. Wang, "E-shaped array antenna with high gain and low profile for 60 GHz applications," in *Proceedings of the 2016 IEEE MTT-S International Microwave Workshop Series on Advanced Materials and Processes for RF and THz Applications (IMWS-AMP)*, pp. 1–3, Chengdu, China, 2016.

[27] M. S. Alam, M. T. Islam, N. Misran, and J. S. Mandeep, "A wideband microstrip patch antenna for 60 GHz wireless applications," *Elektronica and Elektrotechniek*, vol. 19, no. 9, pp. 65–70, 2013.

[28] M. Ur-Rehman, N. A. Malik, X. Yang, Q. H. Abbasi, Z. Zhang, and N. Zhao, "A low profile Antenna for millimeter-wave body-centric applications," *IEEE Transactions on Antennas and Propagation*, vol. 65, no. 12, pp. 6329–6337, 2017.

[29] N. Chahat, M. Zhadobov, L. Le Coq, S. I. Alekseev, and R. Sauleau, "Characterization of the interactions between a 60-GHz antenna and the human body in an off-body scenario," *IEEE Transactions on Antennas and Propagation*, vol. 60, no. 12, pp. 5958–5965, 2012.

[30] S. Razafimahatratra, J. Sarrazin, A. Benlarbi-Delaï et al., "On-body propagation characterization with an H-plane substrate integrated waveguide (SIW) horn antenna at 60 GHz," in *Proceedings of the 2015 European Microwave Conference*, pp. 211–214, Paris, France, 2015.

[31] N. Chahat, M. Zhadobov, L. Le Coq, and R. Sauleau, "Wearable endfire textile antenna for on-body communications at 60 GHz," *IEEE Antennas and Wireless Propagation Letters*, vol. 11, pp. 799–802, 2012.

[32] B. Yeboah-Akowuah, P. Kosmas, and Y. Chen, "A Q-slot monopole for UWB body-centric wireless communications," *IEEE Transactions on Antennas and Propagation*, vol. 65, no. 10, pp. 5069–5075, 2017.

[33] M. M. Khan, K. Islam, M. N. A. Shovon, M. Masud, M. Baz, and M. A. AlZain, "Various textiles-based comparative analysis of a millimeter wave miniaturized novel antenna design for body-centric communications," *International Journal of Antennas and Propagation*, vol. 2021, Article ID 2360440, 14 pages, 2021.

[34] Italian National Research Council, *Dielectric Properties of Body Tissues in the Frequency Range 10 Hz to 100 GHz*Italian National Research Council, Rome, Italy, 2021.